© 2016. Published by The Company of Biologists Ltd | Development (2016) 143, 4608-4619 doi:10.1242/dev.140715

STEM CELLS AND REGENERATION

RESEARCH ARTICLE

PRMT5 is essential for the maintenance of chondrogenic progenitor cells in the limb bud

Jacqueline L. Norrie[1], Qiang Li[1], Swanie Co[1], Bau-Lin Huang[2], Ding Ding[3], Jann C. Uy[1], Zhicheng Ji[3], Susan Mackem[2], Mark T. Bedford[4], Antonella Galli[5], Hongkai Ji[3] and Steven A. Vokes[1,*]

ABSTRACT

During embryonic development, undifferentiated progenitor cells balance the generation of additional progenitor cells with differentiation. Within the developing limb, cartilage cells differentiate from mesodermal progenitors in an ordered process that results in the specification of the correct number of appropriately sized skeletal elements. The internal pathways by which these cells maintain an undifferentiated state while preserving their capacity to differentiate is unknown. Here, we report that the arginine methyltransferase PRMT5 has a crucial role in maintaining progenitor cells. Mouse embryonic buds lacking PRMT5 have severely truncated bones with wispy digits lacking joints. This novel phenotype is caused by widespread cell death that includes mesodermal progenitor cells that have begun to precociously differentiate into cartilage cells. We propose that PRMT5 maintains progenitor cells through its regulation of *Bmp4*. Intriguingly, adult and embryonic stem cells also require PRMT5 for maintaining pluripotency, suggesting that similar mechanisms might regulate lineage-restricted progenitor cells during organogenesis.

KEY WORDS: BMP4, PRMT5, SOX9, Chondrogenesis, Limb development, Progenitor cells

INTRODUCTION

Differentiating cartilage elements are specified from a highly proliferative mesodermal progenitor population that is specified early in limb development. After specification, progenitor cells coalesce into condensates, activate *Sox9*, exit the cell cycle, and subsequently acquire the distinct morphology of chondrocytes (Akiyama et al., 2005; Barna and Niswander, 2007; Benazet et al., 2012; Boehm et al., 2010; Dudley et al., 2002; Pizette and Niswander, 2000). Early condensate growth is not well characterized but includes both localized chondrocyte proliferation and the recruitment of progenitor cells onto their distal ends (Shubin and Alberch, 1986; Stark and Searls, 1973; ten Berge et al., 2008; Thorogood and Hinchliffe, 1975).

Mesodermal progenitor cells are regulated by multiple extrinsic signals. For example, fibroblast growth factors (FGFs), in addition to acting as specification agents, survival factors and motility agents, work in concert with WNT proteins to inhibit differentiation in the distal limb (Cooper et al., 2011; Gros et al., 2010; Lewandowski et al., 2014; Mariani et al., 2008; ten Berge et al., 2008). By contrast, bone morphogenetic proteins (BMPs) drive chondrogenic differentiation and shape the differentiated limb by promoting apoptosis in the anterior and posterior margins as well as within the inter-digit mesenchyme. (Bandyopadhyay et al., 2006; Barna and Niswander, 2007; Capdevila et al., 1999; Kaltcheva et al., 2016; Lopez-Rios et al., 2012; Macias et al., 1997; Pajni-Underwood et al., 2007; Pizette et al., 2001).

In contrast to the known roles for secreted signaling pathways in regulating limb differentiation, the internal pathways by which mesodermal cells maintain a progenitor state are not understood. This process, which appears to involve a timing mechanism regulating histone acetylation, must balance renewal and differentiation in a manner that controls the expansion of differentiated skeletal elements (Rosello-Diez et al., 2014; Saiz-Lopez et al., 2015; Suzuki et al., 2008). Although stem cells differ from progenitor cells in multiple aspects, they both maintain relatively undifferentiated states. With this in mind, we hypothesized that limb bud mesodermal cells maintain progenitor states through a stem cell-like pluripotency pathway. *Prmt5*, which we find is expressed at high levels in the distal limb, is essential for maintaining mouse embryonic and adult stem cell pluripotency and is also required *in vivo* for mouse inner cell mass and primordial germ cell development (Ancelin et al., 2006; Tee et al., 2010). However, owing to the early embryonic lethality of *Prmt5* null mutants, its role has not been explored during organogenesis.

PRMT5 is a member of a family of arginine methyltransferase enzymes. Whereas other members of the pathway monomethylate or asymmetrically dimethylate arginine residues, PRMT5 symmetrically dimethylates arginine residues (reviewed by Bedford and Clarke, 2009; Stopa et al., 2015). Regulating a diverse set of target proteins, it can methylate specific Sm proteins, facilitating their assembly into a core complex of spliceosomal snRNPs (Chari et al., 2008; Meister and Fischer, 2002; Neuenkirchen et al., 2015; Pelz et al., 2015). Additionally, PRMT5 can regulate gene expression by methylation of histones H2A/H4 and H3 (specifically H2A/H4R3 and H3R8), which are generally associated with transcriptional repression (Ancelin et al., 2006; Di Lorenzo and Bedford, 2011; Lee and Bedford, 2002; Tee et al., 2010; Zhang et al., 2015; Zhao et al., 2009).

Here, we show that *Prmt5* is expressed in mesodermal progenitor cells in the limb bud and is essential for their maintenance. Embryos lacking *Prmt5* in their limb buds develop striking defects in skeletal morphogenesis that are caused by early defects in cartilage formation. These defects are caused by widespread apoptosis and precocious differentiation of mesodermal progenitor cells as a consequence of elevated BMP activity. These findings establish an intrinsic mechanism for regulating chondrogenic progenitor cells in

[1]Department of Molecular Biosciences, University of Texas at Austin, 2500 Speedway Stop A4800, Austin, TX 78712, USA. [2]Cancer and Developmental Biology Laboratory, CCR, NCI, Frederick, MD 21702, USA. [3]Department of Biostatistics, Johns Hopkins Bloomberg School of Public Health, 615 North Wolfe Street, Room E3638, Baltimore, MD 21205, USA. [4]Department of Epigenetics & Molecular Carcinogenesis, M.D. Anderson Cancer Center, 1808 Park Road 1C (P.O. Box 389), Smithville, TX 78957, USA. [5]Wellcome Trust Sanger Institute, Hinxton, Cambridge CB10 1SA, UK.

*Author for correspondence (svokes@austin.utexas.edu)

S.A.V., 0000-0002-1724-0102

Received 1 June 2016; Accepted 24 October 2016

Development (2016) 143, 4608-4619 doi:10.1242/dev.140715

the embryo. As *Prmt5* is essential for stem cell pluripotency, our results suggest intriguing similarities between the regulation of tissue-specific progenitor cells and stem cells.

RESULTS

To gain insight into the effects of *Prmt5* on limb development, we first examined its expression pattern in developing mouse embryos. At E11.5, *Prmt5* is dynamically expressed, with high levels of expression in the presomitic mesoderm, craniofacial primordia and, prominently, the limb buds (Fig. 1A). *Prmt5* is uniformly expressed throughout the forelimb and hindlimb buds at E10.5 (Fig. 1B,E) but is much higher in the distal mesenchyme at E11.5 (Fig. 1C,F). By E12.5, *Prmt5* is primarily detected in the distal tip of the developing digit rays (Fig. 1D arrowheads, G), in a region corresponding to the proposed phalanx-forming region (PFR) that provides a progenitor population for the elongating digit condensates (Montero et al., 2008; Suzuki et al., 2008). The progressive distalization of *Prmt5* expression and its absence from chondrogenic condensates indicates that *Prmt5* is largely restricted to undifferentiated limb bud mesoderm. We noted a similar trend for the expression domain of *Mep50* (*Wdr77*), a co-factor that regulates the function of PRMT5 (Antonysamy et al., 2012; Burgos et al., 2015; Saha et al., 2016) (Fig. S1).

Prmt5 conditional mutants have truncated skeletal elements and abnormal digits

Because *Prmt5* null embryos fail to develop past the blastocyst stage (Tee et al., 2010), we conditionally knocked out *Prmt5* in limb buds using a floxed allele along with the limb bud-specific *Prx1Cre* (*Prx1* is also known as *Prrx1*) (Logan et al., 2002). There was a substantial reduction in PRMT5 protein levels in E11.5 limb buds (Fig. S2), as well as a reduction in proteins with symmetrically dimethylated arginine modifications in *Prmt5* conditional knockout forelimbs (Fig. 1H) (Dhar et al., 2013). Whereas *Prx1Cre*$^{+/-}$; *Prmt5*$^{c/+}$ littermates appeared normal, *Prx1Cre*$^{+/-}$; *Prmt5*$^{c/c}$ mice (hereafter referred to as *Prmt5* cKO) had severe, distinctive forelimb defects (Fig. 1I,J), suggesting an essential role for *Prmt5* during limb development.

At E18.5, *Prmt5* cKOs had severely truncated forelimbs (5/5 embryos), with the radius, ulna and humerus each significantly shorter than those of control littermates (Fig. 2A-C). The posterior bone of the forearm contained the olecranon process that is indicative of the ulna, while this process was appropriately absent from the anterior bone (5/5 embryos), suggesting that there were no gross anterior-posterior defects. The deltoid tuberosity was missing from the humerus (4/5 embryos) and the forelimb autopods had substantially reduced numbers of wrist bones (two or three in total; Fig. 2H,H′; *n*=5/5). The digits of the *Prmt5* cKO were irregular, wispy and short, with little or no ossification and a complete absence of joints (Fig. 2G-K). Most *Prmt5* cKO limbs contained four severely truncated digits (4/5 embryos). Based on the size and position of the remaining digits, the missing digit is likely to correspond to digit 1 (the thumb). Digit 1 is also the last condensate to form in limb buds (Zhu et al., 2008) and therefore the most vulnerable to apoptosis. Additionally, the remaining digits are fused in pairs at the base of the digits. In contrast to the severe defects in the forelimbs, *Prmt5* cKO hindlimbs are patterned normally, although the tibia, fibula and femur were all significantly shorter than in control siblings (Fig. 2D-F). The hindlimb autopods were also truncated and most digits were significantly shorter than in the control (Fig. 2L-N). Therefore, in both the forelimb and the hindlimb, *Prmt5* is essential for proper limb outgrowth.

Loss of *Prmt5* results in truncated digit condensates that lack joints

Skeletal truncations can be caused by defects in either chondrogenesis or in subsequent bone formation. To determine the onset of the *Prmt5* cKO phenotype, we analyzed digit formation at E11.5 by *in situ* hybridization for *Sox9*, the earliest known marker of chondrocytes (Akiyama et al., 2005; Bi et al., 1999; Lefebvre and Smits, 2005; Wright, 1995). At this stage, at least two distinct *Sox9*-positive digit rays could be resolved in

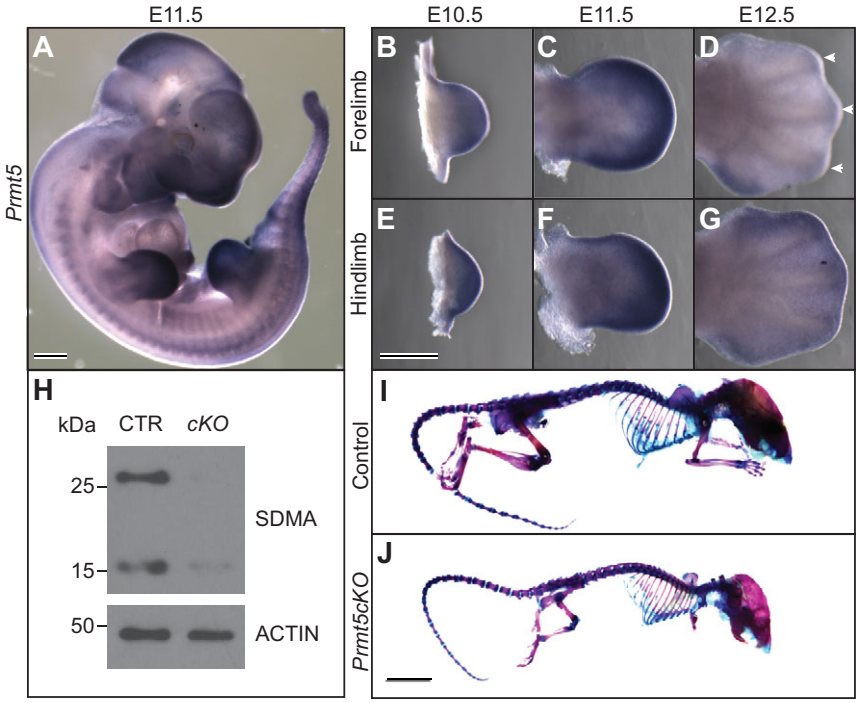

Fig. 1. *Prmt5* is dynamically expressed in undifferentiated limb buds and is essential for their development. (A) Whole-mount *in situ* hybridization for *Prmt5* in an E11.5 mouse embryo showing dynamic regional expression. (B-G) *In situ* hybridization for *Prmt5* in (B-D) forelimbs and (E-G) hindlimbs. Note the distal expression at the tip of the digit condensates at E12.5 (D, arrowheads). (H) Western blot with an SDMA antibody that recognizes proteins that contain symmetrically dimethylated arginines, showing expression in forelimbs of E11.5 control (CTR) and *Prmt5* cKO embryos. (I,J) Skeletal preparations of control and *Prmt5* cKO mice at P21. Scale bars: 500 µm in A,E; 1 cm in J.

Development (2016) 143, 4608-4619 doi:10.1242/dev.140715

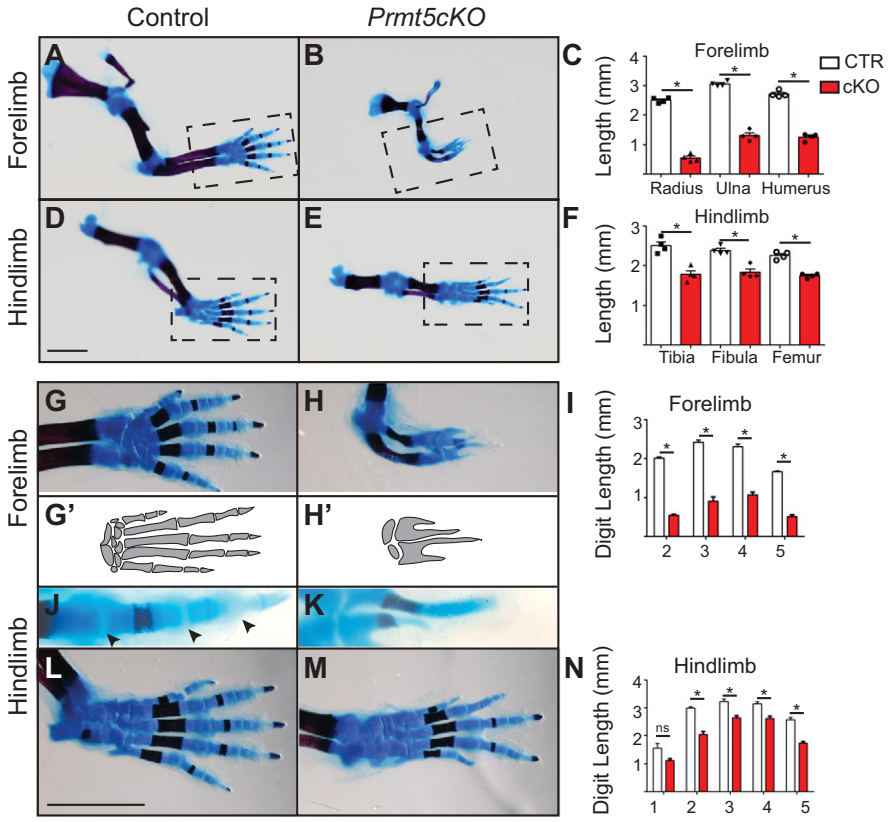

Fig. 2. Conditional loss of *Prmt5* results in severe limb truncations and autopod defects. E18.5 skeletal preparations from control and *Prmt5* cKO forelimbs (A,B) and hindlimbs (D,E). The skeletal elements in both the forelimbs (C) and hindlimbs (F) are significantly reduced in *Prmt5* cKO embryos (n=4 for each). (G,H,L,M) Higher magnifications of the boxed regions in A,B,D,E. (G′,H′) Representative schematics of the autopods from control and *Prmt5* cKO forelimbs. Note the severe reduction in digit length (n=5) and number (n=4/5). (J,K) High magnification of single digits showing the lack of joints (arrowheads in J) in the *Prmt5* cKO. (I,N) Quantification of digit length (mm) using the right limbs from control (n=7) and *Prmt5* cKO (n=5) embryos. *P<0.005 (Student's t-test), for skeletal elements in *Prmt5* cKO versus heterozygous or control siblings; ns, not significant. Error bars indicate s.e.m. Scale bars: 2 mm.

control forelimb buds, whereas *Prmt5* cKO limb buds were slightly smaller, with no resolvable digit rays and a significant increase in the domain of undifferentiated, *Sox9*-negative mesenchyme at the distal tip of the limb bud (Fig. 3A-C,J). Despite the unresolved digit rays and the increase in *Sox9*-negative area, overall SOX9 levels were unchanged (Fig. 3F,G). By E12.5, control embryos have five distinct *Sox9*-expressing digit rays, whereas *Prmt5* cKO limbs are much smaller, with truncated, poorly resolved digit rays (Fig. 3D,E,J).

We also examined the expression of the early joint marker *Gdf5* (Merino et al., 1999b; Storm and Kingsley, 1999). In the control at E12.5, *Gdf5* expression surrounded each digit ray, with additional expression traversing the digit rays, corresponding to the future joints of digits 3 and 4 (Fig. 3H). The *Prmt5* cKO forelimbs had reduced domains of *Gdf5* that did not extend as far distally as in the control (Fig. 3I). As GDF5 is essential for the formation of many joints (Storm and Kingsley, 1999), the reduction might underlie the absence of joints in *Prmt5* cKO forelimbs (Fig. 2H).

We next examined expression of *Col2a1*, a marker of differentiating chondrocytes (Bi et al., 1999). At E13.5, *Prmt5* cKO forelimbs had a significant reduction in digit length, with either four (n=1/3) or five (n=2/3) small, wispy digit outgrowths that tapered distally and lacked any joints (Fig. 3K-M). In all three cases, digit 2 was fused to digit 3 and, in one case, digit 4 was fused to digit 5. Digit 1, if present, was an extremely small single piece of cartilage articulated to the anterior side of the wrist. In the forelimbs with only four digits, it appeared that the anterior articulation was absent. By contrast, and consistent with the much milder phenotype at E18.5, *Prmt5* cKO hindlimbs appeared relatively normal (Fig. 3N,O). Although the digits were on average shorter than control digits, the difference was not statistically significant at this stage (Fig. 3P). We conclude that the phenotypes seen in *Prmt5* cKO limb buds are the result of primary defects in early cartilage specification.

Genomic analysis of *Prmt5* cKO limbs

To obtain insight into the genetic pathways affected by PRMT5, we performed RNA-seq on E11.5 control and *Prmt5* cKO forelimbs (Fig. 4A) and identified 208 differentially expressed genes using stringent conditions (fold-change >2, average FPKM >1 and q-value <0.01; Table S1). We then identified enriched categories using gene ontology (GO) terms (Wang et al., 2013). Top categories included upregulation of apoptotic and BMP signaling genes and the downregulation of genes involved in chondrogenic differentiation (Table S2). In addition, several of the significantly downregulated genes are known to cause human syndromes with short digits (brachydactyly), including *Gdf5*, *Bmpr1b* and noggin (*Nog*) (Al-Qattan et al., 2015; Byrnes et al., 2010; Lehmann et al., 2007, 2003; Ploger et al., 2008).

As PRMT5 can regulate the formation of the spliceosomal complex (Chari et al., 2008; Meister and Fischer, 2002) we also examined the frequency of intron retention in transcripts to determine if introns were retained. We applied a logistic regression model of the ratio of intron to exon counts for genes in control and *Prmt5* cKOs and estimated the odds ratio between the groups. Genes in *Prmt5* cKOs have 1.3-fold higher odds of a read coming from an intron than for the same genes in the control, indicating that the number of retained introns is significantly elevated compared with controls (Fig. 4B). Consistent with this result, there is also a difference in the probability distribution of the intron retention rate (Fig. 4C). Because the differences are small, we believe that the biological significance of this effect is likely to be

Development (2016) 143, 4608-4619 doi:10.1242/dev.140715

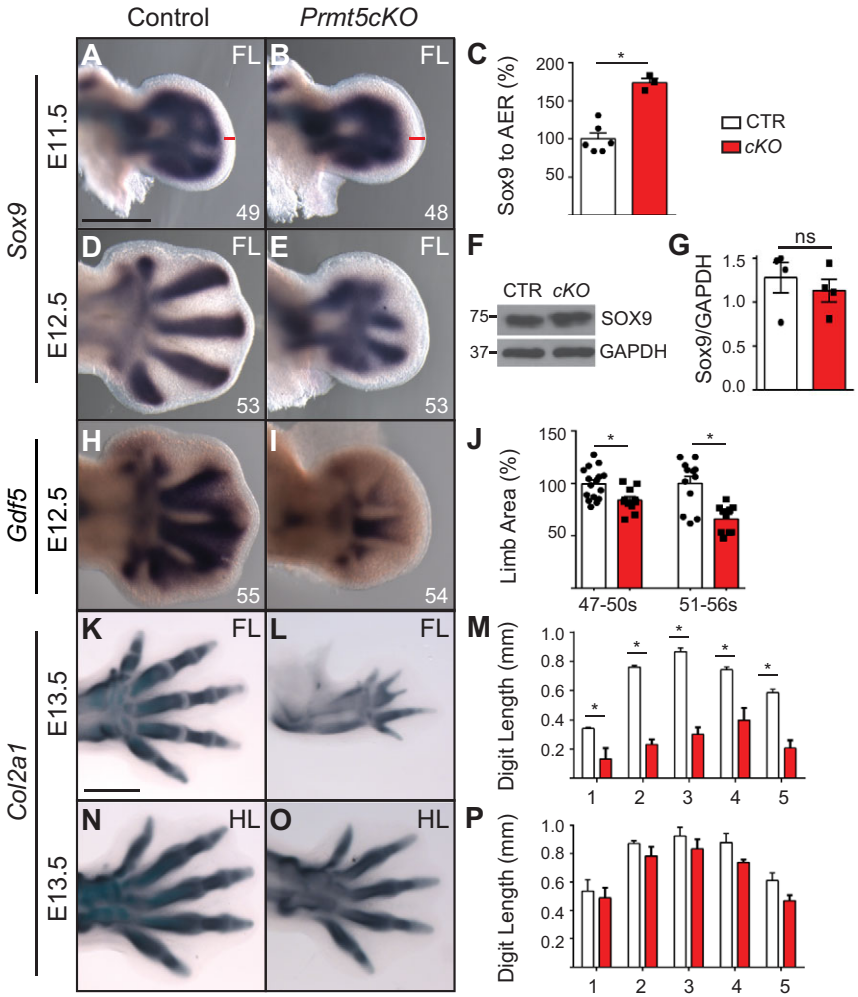

Fig. 3. Abnormal digit ray formation and chondrogenesis in *Prmt5* cKO. (A,B) Whole-mount *in situ* hybridization for *Sox9* in control and *Prmt5* cKO forelimbs (FL) at E11.5. (C) Quantification of the distance from the distal boundary of *Sox9* expression to the distal tip of the forelimb, as indicated by the red bars in A and B, is significantly expanded in E11.5 *Prmt5* cKO embryos (control, *n*=6; *Prmt5* cKO, *n*=3). (D,E) *In situ* hybridization for *Sox9* in control and *Prmt5* cKO forelimbs at E12.5. (F) Western blot showing SOX9 and GAPDH control expression in forelimbs from individual E11.5 embryos and (G) quantification of band intensities, with SOX9 normalized to GAPDH and the dots indicating biological replicates (*n*=4 for both control and *Prmt5* cKO). (H,I) *In situ* hybridization for the joint marker *Gdf5* at E12.5 in control and *Prmt5* cKO forelimbs. (J) *Prmt5* cKO forelimbs occupy a smaller area than controls. Forelimb area is depicted at two different ranges of somite staging (*x*-axis). For the 47-50 somite cohort: control, *n*=16; *Prmt5* cKO, *n*=11. For the 51-56 somite cohort: control, *n*=12; *Prmt5* cKO, *n*=10. (K,L,N,O) E13.5 whole-mount *in situ* hybridizations cleared in benzyl alcohol:benzyl benzoate showing *Col2a1* expression in control and *Prmt5* cKO forelimbs and hindlimbs (HL). The *Prmt5* cKO forelimbs (*n*=3) have dramatic truncations in digit length (M), whereas the hindlimbs (*n*=3) do not have significant reductions in digit length (P). **P*<0.05 (Student's *t*-test), for skeletal elements in *Prmt5* cKO versus heterozygous or control siblings; ns, not significant. Error bars indicate s.e.m. (A,B,D,E,F,I) The number of somites present in the embryo is indicated bottom right. Scale bars: 500 µm.

minimal. Moreover, the transient temporal requirement for PRMT5 in limb bud formation (see proposed model in the Discussion) is not consistent with a significant role in RNA splicing, which would presumably result in a prolonged requirement for PRMT5 during limb formation.

The SHH-FGF loop is unaffected in *Prmt5* cKOs

Owing to the severe limb truncations and high levels of apoptosis observed in limb buds deficient in SHH or apical ectodermal ridge (AER)-derived FGFs (Chiang et al., 2001; Sun et al., 2002; Zhu et al., 2008), we first considered the breakdown of the SHH-FGF feedback loop as a potential cause of the *Prmt5* cKO phenotype. However, several lines of evidence suggest that neither of these pathways is reduced in *Prmt5* cKO limb buds. *Shh*, *Fgf8*, *Spry4* and *Hoxd13* expression levels were either unchanged or slightly upregulated in *Prmt5* cKO forelimbs, both in the RNA-seq data and in independent qRT-PCR experiments (Fig. 4A,D). Moreover, their spatial expression domains are also unaltered (Fig. S3), suggesting that there are no changes in anterior-posterior polarity. Finally, limb buds lacking expression of SHH or FGF4/8 have greater reductions in digit number than *Prmt5* cKO forelimbs, while the remaining digits do not have the brachydactyly or absence of joints observed in *Prmt5* cKO forelimbs (Chiang et al., 2001; Kraus et al., 2001; Sun et al., 2002; Zhu et al., 2008). We conclude that the SHH-FGF loop is intact and largely unaltered in *Prmt5* cKOs.

PRMT5 prevents apoptosis in the distal limb bud

As *Prmt5* cKO limbs had a significant increase in the expression of genes involved in apoptosis (Table S2), we examined the extent of apoptosis in the developing limb. There were no changes in cell death at E10.5, but there was a substantial increase in the number of apoptotic cells in E11.5 *Prmt5* cKO forelimbs (Fig. 5A,D, Figs S4, S5), confirming the RNA-seq results. High levels of apoptosis were sustained at least through E12.5 (Fig. S5G,J). The hindlimb showed no increase in apoptosis at E11.5, and only a slight increase in apoptosis at E12.5 (Fig. S6C,H), consistent with the milder phenotype.

To determine which cells were dying in the forelimb, we examined sections co-stained for cleaved caspase 3 and SOX9 (Fig. 5B,E). Consistent with the spatial expression data (Fig. 3A-C), the SOX9 domain was truncated proximally in *Prmt5* cKOs. The expanded region of distal mesenchyme contained the majority of apoptotic cells located outside the SOX9-expressing cartilage condensates, even extending into the more proximal limb (Fig. 5C,F, Fig. S5). Control embryos rarely expressed SOX9 in the distal limb (an average of four cells per section; *n*=3 embryos; Fig. 5G-I,M), whereas the large majority of apoptotic cells in *Prmt5* cKOs expressed low levels of SOX9 (Fig. 5J-N, Figs S4, S7). These cells did not express COL2, a marker of maturing chondrocytes, suggesting that these cells are in the early stages of chondrogenesis (Fig. S8). The presence of SOX9 in apoptotic cells lying outside the normal condensate domain suggests that the mesodermal progenitor

Development (2016) 143, 4608-4619 doi:10.1242/dev.140715

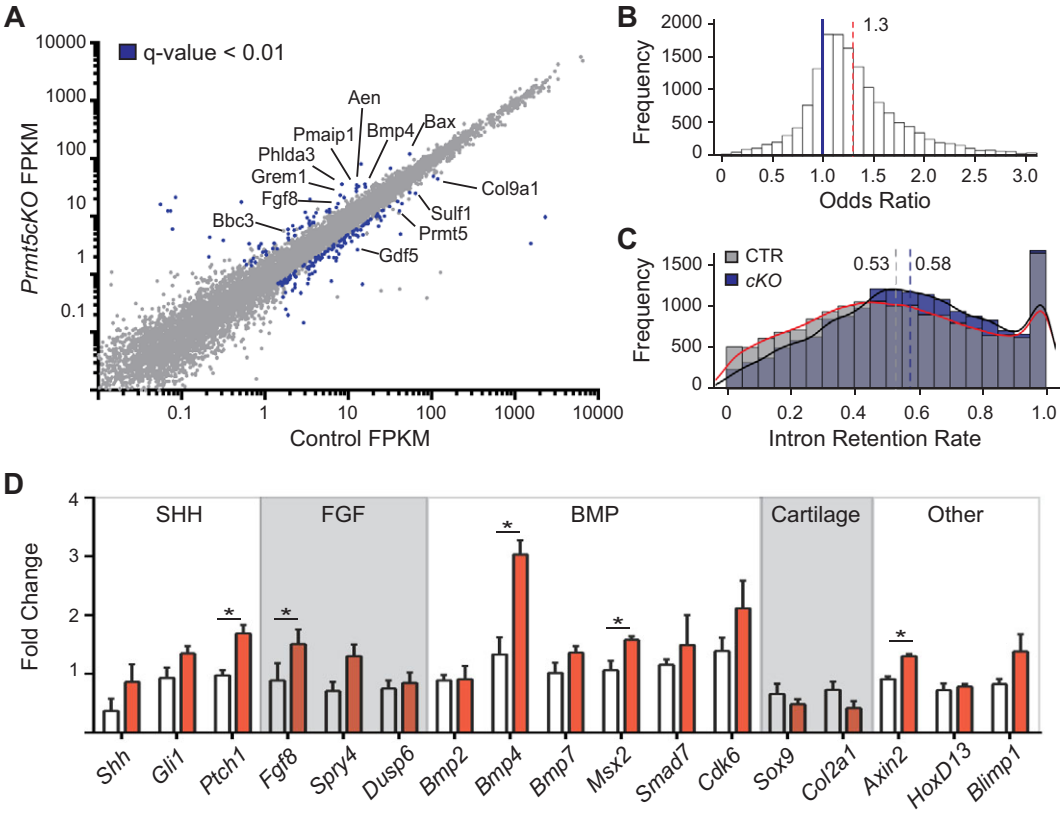

Fig. 4. *Prmt5* cKO limb buds have elevated expression levels for apoptotic pathway genes. (A) Scatter plot of gene expression (FPKM) for *Prmt5* cKO and control RNA-seq data. The blue data points indicate significantly altered genes using a stringent cutoff. (B) The odds ratio [$(\text{intron/exon})_{Prmt5\ cKO}/(\text{intron/exon})_{Control}$] acquired from logistic regression analysis. The odds ratio was 1.30 [95% confidence interval (1.22, 1.38)]. Across all analyzed genes, the average intronic retention is significantly different in *Prmt5* cKOs (one-sample *t*-test, $P<0.001$). (C) Frequency of intron retention rate (intron/gene read count) of all genes for control and *Prmt5* cKO. Average rates are indicated by the dashed lines (control=0.53, *Prmt5* cKO=0.58). (D) qRT-PCR validation of genes in known signaling pathways involved in limb development. FPKM, fragments per kilobase of exon per million fragments mapped. White bars, control; red bars, *Prmt5* cKO. *$P<0.05$ (Student's *t*-test). Error bars indicate s.e.m.

cells undergoing apoptosis are in the process of precociously differentiating into chondrocytes.

Prmt5 cKOs have increased non-canonical BMP signaling

The most upregulated limb patterning gene in the *Prmt5* cKO forelimbs was *Bmp4*, whereas *Bmp2* and *Bmp7* were not significantly altered (Fig. 4D). Consistent with the increased expression levels indicated by RNA-seq and qRT-PCR, there was also a substantial increase in the spatial domain of *Bmp4* in *Prmt5* cKO forelimbs, and later also in hindlimbs (Fig. 6A-D, Fig. S6C,I). *Msx2*, a target of canonical BMP signaling (Lallemand, 2005; Pizette and Niswander, 1999), although slightly upregulated as assessed by independent qRT-PCR (Fig. 4D), was unchanged in RNA-seq analysis and its spatial expression was unaltered (Fig. 6E,F). Moreover, the spatial domain and overall levels of phosphorylated SMAD1,5,8, a direct readout of canonical BMP signaling, were unchanged (Fig. 6G,H, Fig. S6I,J, Fig. S9). Together, these results suggest that there are no substantial alterations in responses to canonical BMP signaling in *Prmt5* cKOs.

As BMP4 activity is regulated on several levels, including negative transcriptional feedback by GREM1 and proteolytic processing of the pro-protein, the increased *Bmp4* expression does not imply an increase in BMP activity (Benazet et al., 2009; Bragdon et al., 2011; Capdevila et al., 1999; Michos et al., 2004; Norrie et al., 2014). To establish if there is a biologically relevant increase in BMP activity in *Prmt5* cKO hindlimbs, we crossed *Prmt5* cKOs into $Rosa^{Gremlin/+}$, a Cre-inducible line that activates *Grem1*. GREM1 binds to and sequesters BMP ligands, resulting in a reduction in overall BMP activity by over 50% (Hsu et al., 1998; Norrie et al., 2014). As a consequence of reduced BMP activity, there is an early failure of forelimb initiation, while the hindlimbs have fully penetrant polydactyly with decreased apoptosis (Norrie et al., 2014). We reasoned that if BMP4 activity was increased in *Prmt5* cKO hindlimb buds, it might rescue the hindlimb polydactyly caused by reduced BMP levels. We did not expect to rescue the forelimb outgrowth defect in $Prx1Cre^{+/-}$; $Rosa^{Gremlin/+}$ embryos, as this is caused by an early failure in limb outgrowth that would precede *Prmt5* inactivation (Norrie et al., 2014). As expected, control and *Prmt5* cKO littermates had five hindlimb digits, whereas $Rosa^{Gremlin/+}$ embryos had polydactyly with an average of 6.8 digits. Compared with $Prx1Cre^{+/-}$; $Rosa^{Gremlin/+}$ embryos, $Prx1Cre^{+/-}$; $Rosa^{Gremlin/+}$; *Prmt5* cKO embryos had a significant rescue in digit number (5.5 digits, $n=6$; Fig. 6I-M). We conclude that the increased *Bmp4* expression results in increased BMP4 activity that can offset hindlimb polydactyly caused by reductions in BMP activity.

BMP signaling has well-established roles in driving apoptosis in the inter-digit mesenchyme and, consequently, the increased BMP activity in *Prmt5* cKO limbs is likely to drive apoptosis (Bandyopadhyay et al., 2006; Buckland et al., 1998; Ganan et al., 1996; Kaltcheva et al., 2016; Merino et al., 1999a; Pajni-Underwood et al., 2007). Prior to inter-digit apoptosis, the application of BMP-containing beads to earlier limb buds causes

Development (2016) 143, 4608-4619 doi:10.1242/dev.140715

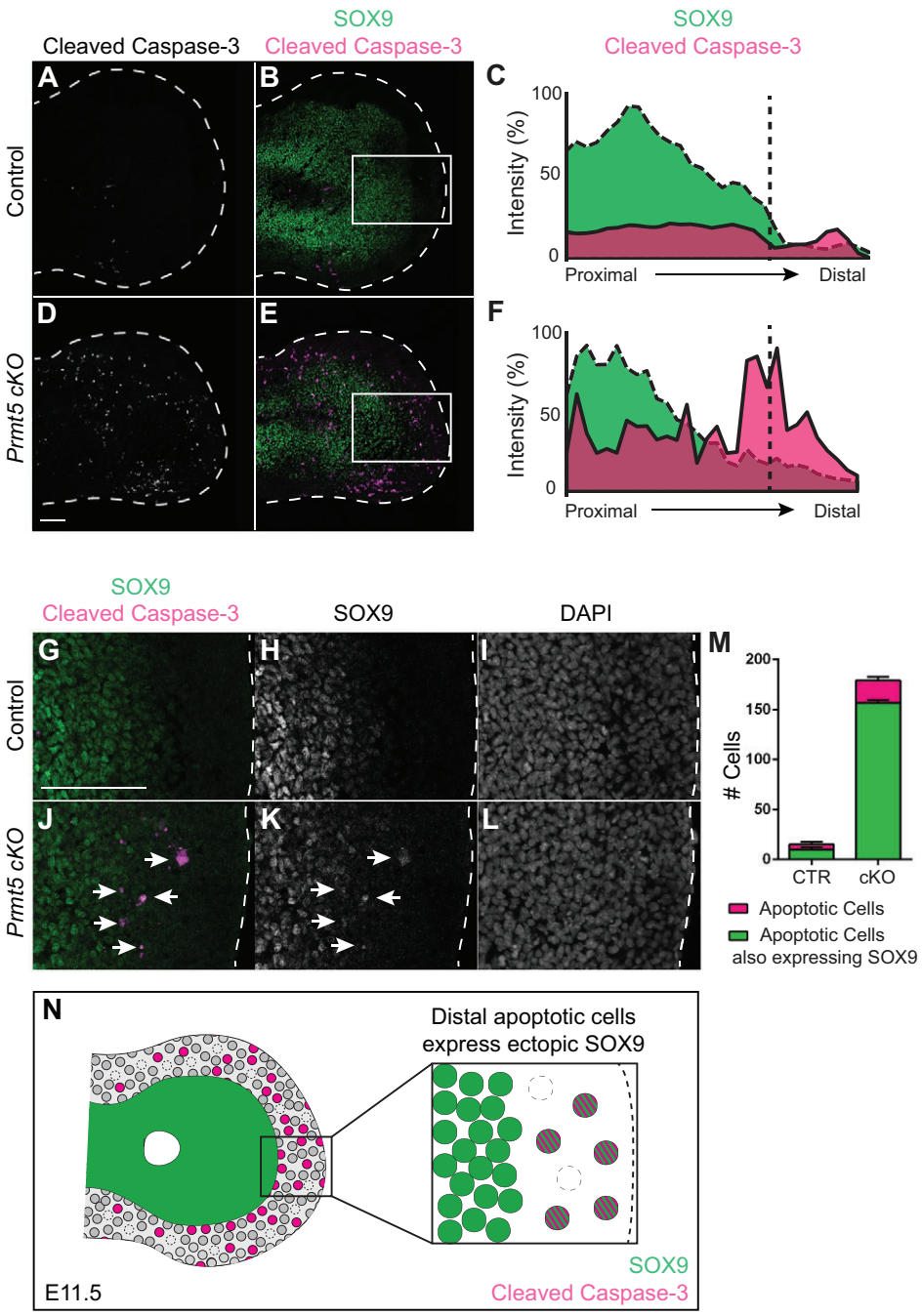

Fig. 5. *Prmt5* cKO limb buds have elevated apoptosis and precocious differentiation in the distal limb bud. Immunostaining for cleaved caspase 3 (A,D) and double staining for cleaved caspase 3 (pink) and SOX9 (green) (B,E) in control and *Prmt5* cKO limb buds at E11.5. (C,F) Quantification of fluorescence intensity for cleaved caspase 3 and SOX9 in control (C) and *Prmt5* cKOs (F) from the distal region as demarcated by the boxes in B and E, respectively. Dashed lines indicate the distal boundary, where SOX9 expression drops below 20% intensity in the control embryo. (G,J) High magnification of SOX9 and cleaved caspase 3 double staining. Arrows indicate double-positive cells. (H,K) SOX9 channel and (I,L) DAPI staining. (M) Quantification of cleaved caspase 3-positive cells that co-express SOX9 in autopod regions of control and *Prmt5* cKO limbs. Maximum intensity projections of three biological replicates were quantified for control and Prmt5 cKOs. Error bars indicate s.e.m. (N) Depiction of the widespread apoptosis in the distal region of *Prmt5* cKO limb buds. Cells currently undergoing apoptosis co-express SOX9 and cleaved caspase 3, and the location of cells that have undergone apoptosis is indicated by dashed outlines. Note the lack of apoptosis in differentiating chondrocytes. Scale bars: 50 µm.

widespread apoptosis in uncondensed mesoderm but does not affect condensed digit rays (Ganan et al., 1996; Macias et al., 1997). Consistent with this, the majority of apoptosis in *Prmt5* cKOs occurs outside the differentiating chondrocyte domain. As canonical BMP signaling was not noticeably upregulated, we analyzed levels of phosphorylated p38 (MAPK14), which mediates a branch of non-canonical BMP signaling (Derynck and Zhang, 2003; Kondo et al., 2014; Kuroyanagi et al., 2015). There was a significant upregulation of phospho-p38 in *Prmt5* cKO forelimbs but not hindlimbs (Fig. 6N,O, Fig. S6D,E), suggesting that the upregulation of BMP4 activates non-canonical p38 signaling. Although the mechanisms underlying the activation of p38 by non-canonical BMPs are not completely understood, the non-canonical and canonical pathways are mutually antagonistic and, in osteoblasts, can toggle between pathways (Feng and Derynck, 2005; Kimura et al., 2000; Kua et al., 2012; Lo et al., 2001; Sapkota et al., 2007). This mutual antagonism provides an explanation for the observed lack of upregulated pSMAD signaling in embryos with upregulated p38. To determine the effect of phospho-p38 on limb differentiation, we added the p38 inhibitor SB203580 (Barančík et al., 2001; Chen et al., 2016; Engel et al., 2005; Hirose et al., 2003; Kim et al., 2016; Tong et al., 1997; Wang et al., 2012) to micromass cultures. After 48 h, control cells had formed nodules, an early step in chondrogenesis that precedes Alcian Blue staining (Barna and Niswander, 2007; Paulsen and Solursh, 1988), whereas the inhibitor-treated cells failed to do so (n=4/4; Fig. S10). This result, which is consistent with previous studies on p38 signaling in chondrogenesis, indicates that p38 signaling is important for

Development (2016) 143, 4608-4619 doi:10.1242/dev.140715

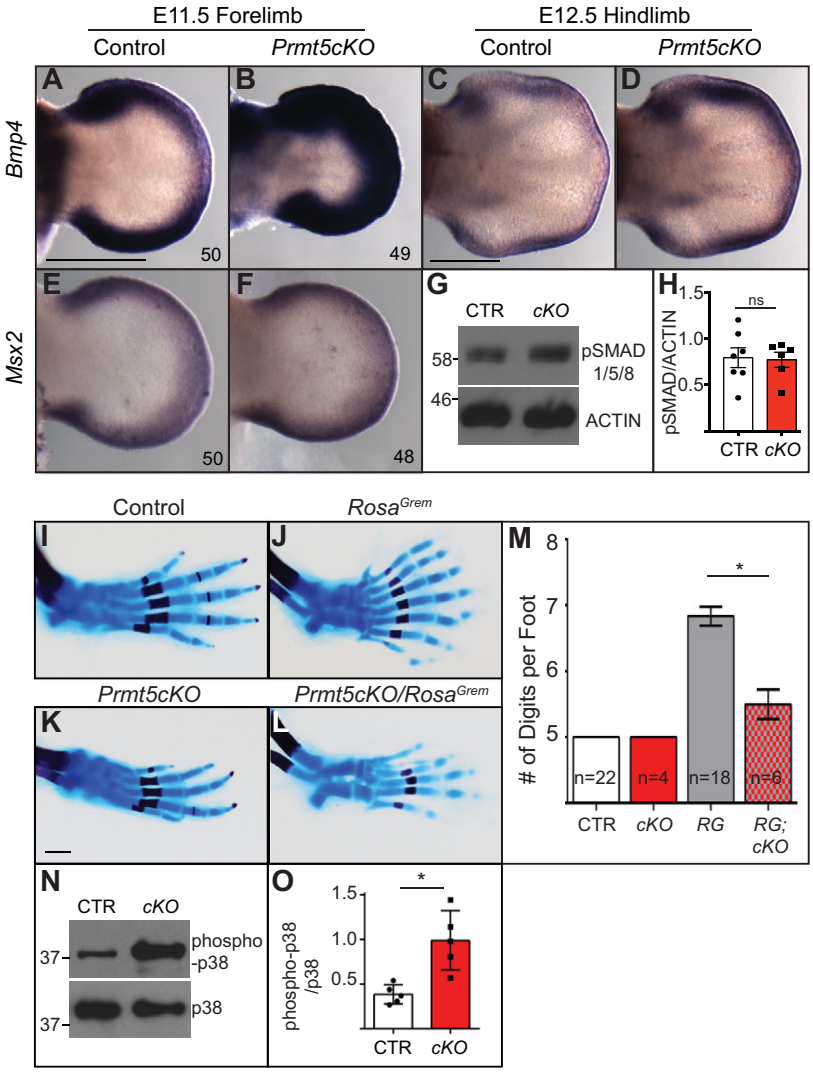

Fig. 6. *Prmt5* cKO limb buds have upregulated BMP activity and elevated levels of phospho-p38. (A,B) *In situ* hybridization of *Bmp4* in control and *Prmt5* cKO forelimbs at E11.5 (50 and 49 somites) and (C,D) hindlimbs at E12.5. (E,F) *In situ* hybridization of *Msx2* in control and *Prmt5* cKO forelimbs at E11.5 (50 and 48 somites). (G) Western blot showing pSMAD1/5/8 and actin control in forelimbs from individual E11.5 embryos and (H) quantification of band intensities, with pSMAD1/5/8 normalized to actin. Control, *n*=7; *Prmt5* cKO, *n*=6. (I-L) E18.5 skeletal preparations of hindlimbs of the specified genotypes. (M) Digit number for each hindlimb of embryos of the specified genotypes. Control, *n*=22; *Prmt5* cKO, *n*=4; *Rosa*^{Gremlin} (RG), *n*=18; *Rosa*^{Gremlin}; *Prmt5* cKO, *n*=6. (N) Western blot showing phospho-p38 and pan-p38 control (blot was stripped and reprobed for pan-p38) in forelimbs from individual E12.5 embryos and (O) quantification of band intensities, with phospho-p38 normalized to pan-p38. Control, *n*=5; *Prmt5* cKO, *n*=5. **P*<0.01 (Student's *t*-test), *Prmt5* cKO compared with heterozygous or control siblings. Error bars indicate s.e.m. Scale bars: 500 µm.

chondrogenesis, and thus the upregulation of phospho-p38 in the *Prmt5* cKO might play a role in the precocious differentiation of the distal mesenchyme (Braem et al., 2012; Nakamura et al., 1999).

DISCUSSION

The conditional deletion of *Prmt5* confers a striking limb phenotype. All skeletal elements in the forelimbs are truncated, with wispy digits that lack joints, whereas the hindlimbs are less severely affected. Underlying the phenotype is widespread apoptosis throughout the undifferentiated mesenchyme that occurs without obvious perturbations to the SHH-FGF loop. The majority of the apoptotic cells are located distal to the SOX9-expressing cartilage condensates but nonetheless precociously express low levels of SOX9. This suggests that they have begun to prematurely differentiate into chondrocytes, perhaps because of heightened BMP activity. We conclude that PRMT5 has an intrinsic role in maintaining progenitor cells in the limb bud.

Enhanced, non-canonical BMP activity in *Prmt5* cKOs

As *Bmp4* expression is negatively regulated by BMP activity, the observed increase in gene expression does not in itself imply enhanced activity (Khokha et al., 2003; Michos et al., 2004; Norrie et al., 2014). The BMP target gene *Msx2* (Lallemand et al., 2005; Pizette and Niswander, 1999), although slightly upregulated in independent qRT-PCR experiments (Fig. 4D), was unchanged in the RNA-seq analysis and does not show consistently expanded spatial expression (Fig. 6E,F). In addition, there was no detectable increase in pSMAD1,5,8 levels, either quantitatively or spatially (Fig. 6G,H, Fig. S7; see below for discussion on SOX9 induction). Nonetheless, *Prmt5* cKOs are able to rescue the hindlimb polydactyly phenotype present in a *Rosa*^{Gremlin} background that is caused by extracellular sequestration of BMP ligands. Blocking BMP ligand activity will result in inhibition of both canonical and non-canonical BMP signaling. As forelimbs of *Rosa*^{Gremlin} embryos have an early defect in AER formation that results in a near complete block to limb outgrowth (Norrie et al., 2014), the later BMP4 upregulation in *Prmt5* cKO forelimbs would occur after the early defect and would therefore be incapable of rescuing the early phenotype.

The p38 mitogen-activated protein kinase (MAPK) pathway, a mediator of the non-canonical BMP response, is substantially elevated in *Prmt5* cKOs. Inhibition of p38 activity inhibits the formation of nodules in micromass cultures (Fig. S10). This is consistent with previous reports (Braem et al., 2012; Nakamura et al., 1999) suggesting that p38-mediated signaling regulates an early step in the chrondrogenic pathway. In several other contexts, BMPs can activate apoptosis through the p38 pathway (Cuadrado et al., 2007; Fukuda et al., 2006; Hay et al., 2001; Kendall et al.,

Development (2016) 143, 4608-4619 doi:10.1242/dev.140715

2005; Kondo et al., 2014; Kuroyanagi et al., 2015; Lafont et al., 2015; Tian et al., 2012). A recent study found that BMPs directly regulate apoptosis in inter-digit limb mesenchyme through an unidentified non-canonical pathway (Kaltcheva et al., 2016). Based on these findings, it is possible that p38 also mediates apoptosis in *Prmt5* cKOs.

PRMT5 is essential for the maintenance of chondrocyte progenitor cells

The majority of apoptotic cells in *Prmt5* cKOs lie within undifferentiated, uncondensed mesoderm that is distal to the normal SOX9-expressing domains (Fig. 5D-F). In control embryos, there is a near complete absence of cells in this region that express SOX9 above background levels. In contrast to their neighboring non-apoptotic cells, the apoptotic cells express low but distinct levels of SOX9 (Fig. 5J-L). The abnormal expression of SOX9 suggests that the uncondensed mesenchymal cells are undergoing precocious differentiation. As low levels of BMP signaling are essential for activating chondrogenesis and *Sox9* in the distal mesoderm (Bandyopadhyay et al., 2006; Benazet et al., 2012; Norrie et al., 2014; Pizette and Niswander, 2000), the elevated levels of BMP activity in *Prmt5* cKOs could result in the activation of precocious *Sox9* in a subset of cells that either concomitantly or subsequently undergo apoptosis. A caveat to this interpretation is that *Sox9* induction in this region of the limb bud requires the canonical BMP signaling component SMAD4 (Benazet et al., 2012). Although we do not detect elevated pSMAD levels that are indicative of enhanced canonical BMP signaling, we speculate that *Prmt5* cKO limb buds nonetheless express mild and/or transient increases in canonical BMP activity that were not detectable in our experiments. Consistent with this possibility, the activation of *Sox9* occurs even in conditions that substantially reduce BMP signaling activity in limb buds (Bandyopadhyay et al., 2006; Norrie et al., 2014). Finally, the role of p38 in chondrogenic differentiation remains uncharacterized, and it remains possible that it could activate *Sox9* in a parallel pathway to that of canonical BMP signaling.

We propose the following model for PRMT5-directed maintenance of progenitor cells in the forelimb. In normal conditions, PRMT5 inhibits *Bmp4*, thereby promoting survival and continued proliferation of progenitor cells while inhibiting their differentiation into chondrocytes. In the absence of PRMT5, an upregulation of *Bmp4* triggers apoptosis through non-canonical BMP signaling. Sustained high levels of apoptosis in the progenitor population deplete progenitor cells, resulting in fewer chondrocytes, which will eventually condense and differentiate into severely truncated limbs and often lead to a reduction in digits (Fig. 7). Despite clear defects, *Prmt5* cKOs have an extensive degree of forelimb development, a result that initially seems at odds with an absolute requirement for PRMT5 in maintaining limb progenitor cells. The comparatively normal hindlimbs provide an explanation for this, as the *Prx1Cre* transgene has a delayed onset of activity in the hindlimb compared with the forelimb (Logan et al., 2002), resulting in the prolonged expression of PRMT5 in the hindlimb. The difference in timing suggests that an early pulse of PRMT5 activity in the forelimb is sufficient for a considerable degree of limb development, while a slightly more prolonged exposure results in a nearly normally patterned hindlimb. This is consistent with the notion that PRMT5 has a fundamental role in maintaining the transient population of limb progenitors.

The expression of *Prmt5* becomes progressively restricted to undifferentiated limb mesoderm, and is finally expressed in the uncondensed mesoderm distal to the digit ray (arrowheads in Fig. 1D). This region corresponds to the PFR, an uncondensed progenitor region expressing SOX9 that gives rise to progressively more distal digit elements (Montero et al., 2008; Suzuki et al., 2008; Witte et al., 2010). The loss of this region could contribute to the truncated, unarticulated digits in *Prmt5* cKOs. Digit truncation could be occurring analogously to that in $Nog^{-/-}$ embryos, in which BMP levels are also elevated (Brunet et al., 1998). Both *Prmt5* cKO and $Nog^{-/-}$ embryos have truncated digits that lack joints. However, $Nog^{-/-}$ embryos have normal numbers of digits (and even occasionally ectopic cartilage elements) that are thick and stubby, contrasting with the wispy digits in *Prmt5* cKOs. It is presently unknown whether $Nog^{-/-}$ autopods undergo apoptosis, and future studies will be required to clarify whether the truncated digits are primarily caused by an inability to form articulated phalanges or by the depletion of a progenitor pool.

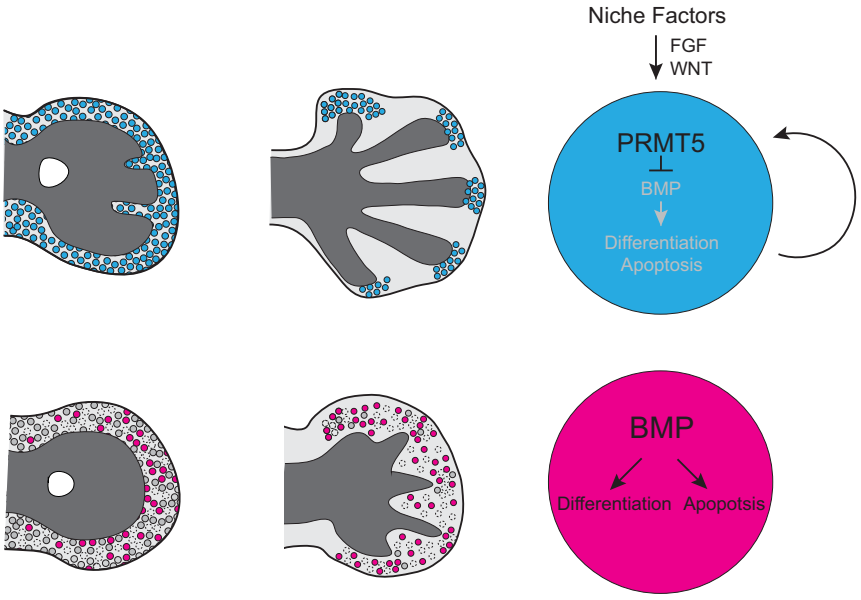

Fig. 7. PRMT5 is essential for maintaining chondrocyte progenitor cells. During normal limb development (top), undifferentiated progenitor cells express PRMT5, which inhibits *Bmp4*, thereby promoting cell survival and limiting differentiation. *Prmt5*-expressing cells are progressively restricted to the distal tip of the developing digit rays, where they probably continue to serve as a progenitor population to the digits. In the absence of PRMT5 (bottom), widespread apoptosis depletes the pool of chondrocyte progenitor cells, resulting in truncated skeletal elements. Without *Prmt5*, an upregulation of *Bmp4* drives precocious differentiation and apoptosis.

Development (2016) 143, 4608-4619 doi:10.1242/dev.140715

PRMT5-mediated mechanisms for maintaining progenitor cells

How is *Prmt5* itself regulated? Co-administration of FGF8 and WNT3A is sufficient to maintain cultured limb bud mesenchyme in a distal, undifferentiated state, and this is likely to reflect the endogenous role of these proteins (Cooper et al., 2011; ten Berge et al., 2008). It is tempting to speculate that they could maintain the expression of *Prmt5*, which would then act as a downstream effector. We note that *Prmt5* is expressed in the mesenchyme underlying *Fgf8* expression in the AER, which also becomes restricted to the distal tips of the digit rays during later development (Lu, 2006). Alternatively, differentiation factors might repress *Prmt5*, restricting its expression and subsequent activity to progenitor cell populations. Although we favor the first model, additional experiments will be necessary to determine if and how external signaling factors regulate *Prmt5*.

PRMT5 maintains chondrocyte progenitor cells at least in part by repressing BMP4-mediated differentiation. PRMT5 directly interacts with several repressors, including SKI and BLIMP1 (Ancelin et al., 2006; Bedford and Clarke, 2009). Although *Blimp1* (*Prdm1*) is required for development of the posterior limb bud, the mutant phenotype is different from that of *Prmt5* cKOs (Robertson et al., 2007), implying a different mechanism of regulation. In several stem cell populations, PRMT5 helps maintain pluripotency by inhibiting differentiation factors (Ancelin et al., 2006; Nagamatsu et al., 2011; Tee et al., 2010), suggesting that a similar mechanism could be regulating both stem cells and progenitor cells within the limb bud during development. Interestingly, an *in vivo* population of *Grem1*-expressing mesenchymal skeletal stem cells was recently identified that has the potential to give rise to bone and cartilage in postnatal animals (Worthley et al., 2015). Although this population is not active in embryos, it highlights a central role for BMP suppression in both embryonic and adult progenitor populations.

MATERIALS AND METHODS

Mouse strains and crosses

Experiments involving mice were approved by the Institutional Animal Care and Use Committee at the University of Texas at Austin (protocol AUP-2013-00,168).

A *Prmt5* conditional mouse line, $Prmt5^{tm2c(EUCOMM)Wtsi}$ (referred to as $Prmt5^{c}$), was crossed with $Prx1Cre1^{+/-}$ males (Logan et al., 2002) to generate $Prx1Cre^{+/-}$; $Prmt5^{c/+}$ males. These were crossed with $Prmt5^{c/c}$ females to generate $Prx1Cre^{+/-}$; $Prmt5^{c/c}$ embryos (*Prmt5* cKOs). *Prmt5* alleles were detected with primers 5′-TGGAACTGCAGGCATATGCC-3′ and 5′-TTCTGGCCTCCATGGGGGAA-3′, generating a 465 bp fragment for the conditional allele and a 247 bp fragment for the wild-type allele. $Prmt5^{c/c}$ females were crossed with $Gt(ROSA)26Sor^{tm1(Grem1)Svok}$ mice (referred to as $Rosa^{Gremlin}$) (Norrie et al., 2014) to generate $Prmt5^{c/+}$; $Rosa^{Gremlin/+}$ mice that were subsequently crossed to $Prx1Cre^{+/-}$; $Prmt5^{c/+}$ mice to generate $Prx1Cre^{+/-}$; $Prmt5^{c/c}$; $Rosa^{Gremlin/+}$ embryos.

Embryonic manipulations

Skeletal preparations were performed as previously described (Allen et al., 2011). Limb skeletal elements were imaged with a Canon EOS Rebel T2i with macro lens or on a Leica M165 stereo microscope and quantified using ImageJ (NIH). Lysotracker Red (Invitrogen L7528) staining on whole-mount limb buds was used as previously described (Fogel et al., 2012; Zhu et al., 2008), with an adjusted Lysotracker Red incubation time of 5 min. Limbs were visualized after clearing in 1:2 benzyl alcohol:benzyl benzoate.

Micromass culture

The effect of phospho-p38 on limb differentiation was assessed in micromass cultures as described in the supplementary Materials and Methods.

Western blots and immunostaining

Limb buds were homogenized in RIPA buffer (5 mM Tris pH 7.5, 150 mM NaCl, 0.1% SDS, 0.5% sodium deoxycholate, 1% Triton X-100) containing complete mini EDTA-free protease inhibitor and PhosphoSTOP (Roche). Approximately 15-20 µg lysate was resolved on 8% (or 15% for anti-SDMA) SDS-PAGE gels, transferred to PVDF membranes (or nitrocellulose for anti-pSMAD1,5,8) and incubated overnight at 4°C with primary antibody. Primary antibodies include: anti-PRMT5 (1:500, 07-405 Cell Signaling Technology), anti-pSMAD1,5,8 (1:500, 9511 Cell Signaling Technology), anti-p38 (1:2500, ab170099 Abcam), anti-phospho-p38 (1:1000, 4511 Cell Signaling Technology), anti-GAPDH (1:1000, 2118 Cell Signaling Technology), anti-actin (1:2000, A2066 Sigma) and anti-SDMA (2C3D6, 1:500) (Dhar et al., 2013). Membranes were then incubated in donkey anti-rabbit secondary antibody (1:2000, 711-035-152 Jackson ImmunoResearch) for 1 h at room temperature and developed using ECL Prime Western Blotting Detection Reagent (GE Healthcare). Band intensities were quantified using ImageJ.

Prior to immunostaining, limb buds were fixed for 20 min at room temperature in 4% paraformaldehyde (PFA). Cryosections (16 µm) were stained with anti-cleaved caspase 3 (1:250, 9664 Cell Signaling Technology) overnight at 4°C followed by anti-SOX9 Alexa Fluor 488 conjugate (1:250, AB5535-AF488 Millipore) for 1 h at room temperature. TUNEL staining was performed using the In Situ Cell Death Detection Kit, Fluorescein (11684795910 Roche), incubating sections for 1 h at room temperature. They were then incubated overnight at 4°C with anti-SOX9 (1:200, AB5535 Millipore). Sections were then incubated with Alexa Fluor 568 goat anti-rabbit secondary antibody (1:250, A11036 Life Technologies) for 1 h at room temperature, and DAPI (300 nM, Life Technologies).

With the exception of pSMAD1,5,8 (see below), limb sections were imaged on a Zeiss 710 confocal microscope collected as tile scans with a 20× objective using a total of four *z*-stacks over a 6 µm range. Higher magnification was acquired on a Zeiss LSM 700 confocal as tile scans with a 40× objective using five *z*-stacks over a 4.8 µm range. Images were processed using ZEN software (Zeiss) into maximum intensity projections and fluorescence intensity was quantified using ImageJ.

Embryos for pSMAD1,5,8 immunostaining were fixed in 4% PFA for 3 h at room temperature then transferred to 70% ethanol. Samples were subsequently Vibratome sectioned (100 µm), incubated with primary antibody (as above, 1:100) overnight at 4°C, and then incubated with Alexa Fluor 594 secondary antibody (1:250, A11037 Invitrogen) for 4 h at room temperature. Images were taken on a Zeiss LSM 710 confocal at 63× magnification, stitched and processed to indicate maximum intensity projections.

COL2 immunostaining of sections is described in the supplementary Materials and Methods.

Quantitative RT-PCR

RNA was extracted using Trizol reagent (15596-026 Life Technologies) and DNase treated. 500 ng RNA was used for cDNA synthesis using SuperScript II reverse transcriptase (18064-014 Invitrogen) with random hexamers. qRT-PCR was performed using SensiFast SYBR Lo-Rox (Bioline) on a Viia 7 (ABI) platform. Values were normalized to β-actin. Fold-change was calculated using the $2^{-\Delta\Delta CT}$ method. qRT-PCR primers are listed in Table S3.

RNA-seq and intron analysis

RNA from three control and two *Prmt5* cKO forelimbs were pair-end sequenced on an Illumina HiSeq 2500 platform. On average we obtained over 26 million aligned pairs per sample. Reads were analyzed using FastQC (Babraham Bioinformatics) and sequences were trimmed to 100 bp using the FASTX-Toolkit (http://hannonlab.cshl.edu/fastx_toolkit). Trimmed sequences were aligned to the mouse mm10 genome using TopHat 2.0.10 (with Bowtie 2.1.0) (Trapnell et al., 2012). Aligned reads were assembled, merged, and tested for differential expression using Cufflinks 2.1.1 (Trapnell et al., 2012). Differential expression data were analyzed in R using CummeRbund (www.rstudio.com; Trapnell et al., 2012). We chose genes with fold-change >2, average FPKM >1 and q-value <0.01 (Storey and Tibshirani, 2003) in expression between control and *Prmt5* cKO (208

Development (2016) 143, 4608-4619 doi:10.1242/dev.140715

genes) for GO analysis. RNA-seq datasets are deposited at GEO (GSE79487).

To identify retained introns, we first identified genes with two or more exons and mapped sequencing reads to their defined exonic and intronic regions using mouse mm10 'TxDb.Mmusculus.UCSC.mm10.knownGene' (R package version 3.2.2). For each gene, we assumed that the read count of intron X followed a binomial distribution with parameters n and p. We then calculated X~B(n,p), where n is the total read count of the gene and p is the probability that a read came from an intron. We fit this to a logistic regression model to estimate the coefficient β_1 by $\log(p/(1-p))=\beta_0+\beta_1$*group, where group is 0 for control and 1 for *Prmt5* cKO. Based on this model, changing the genetic background from control to *Prmt5* cKO would increase the odds of a read coming from an intron by $e^{\beta 1}$-fold.

Acknowledgements

We thank Dr Mark Lewandoski for sharing unpublished data; Dr Blerta Xhemalce for helpful discussions; and Dr Cliff Tabin, Dr John Wallingford and Rachel Lex for comments on the manuscript.

Competing interests

The authors declare no competing or financial interests.

Author contributions

J.L.N., Q.L., D.D., Z.J., S.M., M.T.B., A.G., H.J. and S.A.V. designed the experiments. J.L.N., Q.L., S.C., J.C.U., B.-L.H., D.D., Z.J. and A.G. conducted the experiments. J.L.N., D.D., Z.J., H.J. and S.A.V. wrote the manuscript with input from all authors.

Funding

This work was supported by the National Institutes of Health [R01HD073151 to S.A.V.] and Cancer Prevention Research Institute of Texas [#RP120343 to S.A.V.]. Deposited in PMC for release after 12 months.

Data availability

RNA-seq datasets for *Prmt5* cKO versus control forelimbs are available at Gene Expression Omnibus under accession number GSE79487.

Supplementary information

Supplementary information available online at
http://dev.biologists.org/lookup/doi/10.1242/dev.140715.supplemental

References

Akiyama, H., Kim, J.-E., Nakashima, K., Balmes, G., Iwai, N., Deng, J. M., Zhang, Z., Martin, J. F., Behringer, R. R., Nakamura, T. et al. (2005). Osteo-chondroprogenitor cells are derived from Sox9 expressing precursors. *Proc. Natl. Acad. Sci. USA* **102**, 14665-14670.

Allen, B. L., Song, J. Y., Izzi, L., Althaus, I. W., Kang, J.-S., Charron, F., Krauss, R. S. and McMahon, A. P. (2011). Overlapping roles and collective requirement for the coreceptors GAS1, CDO, and BOC in SHH pathway function. *Dev. Cell* **20**, 775-787.

Al-Qattan, M. M., Al-Motairi, M. I. and Al Balwi, M. A. (2015). Two novel homozygous missense mutations in the GDF5 gene cause brachydactyly type C. *Am. J. Med. Genet. A* **167**, 1621-1626.

Ancelin, K., Lange, U. C., Hajkova, P., Schneider, R., Bannister, A. J., Kouzarides, T. and Surani, M. A. (2006). Blimp1 associates with Prmt5 and directs histone arginine methylation in mouse germ cells. *Nat. Cell Biol.* **8**, 623-630.

Antonysamy, S., Bonday, Z., Campbell, R. M., Doyle, B., Druzina, Z., Gheyi, T., Han, B., Jungheim, L. N., Qian, Y., Rauch, C. et al. (2012). Crystal structure of the human PRMT5:MEP50 complex. *Proc. Natl. Acad. Sci. USA* **109**, 17960-17965.

Bandyopadhyay, A., Tsuji, K., Cox, K., Harfe, B. D., Rosen, V. and Tabin, C. J. (2006). Genetic analysis of the roles of BMP2, BMP4, and BMP7 in limb patterning and skeletogenesis. *PLoS Genet.* **2**, e216.

Barančík, M., Boháčová, V., Kvačkajová, J., Hudecová, S., Križanová, O. and Breier, A. (2001). SB203580, a specific inhibitor of p38-MAPK pathway, is a new reversal agent of P-glycoprotein-mediated multidrug resistance. *Eur. J. Pharm. Sci.* **14**, 29-36.

Barna, M. and Niswander, L. (2007). Visualization of cartilage formation: insight into cellular properties of skeletal progenitors and chondrodysplasia syndromes. *Dev. Cell* **12**, 931-941.

Bedford, M. T. and Clarke, S. G. (2009). Protein arginine methylation in mammals: who, what, and why. *Mol. Cell* **33**, 1-13.

Benazet, J.-D., Bischofberger, M., Tiecke, E., Goncalves, A., Martin, J. F., Zuniga, A., Naef, F. and Zeller, R. (2009). A self-regulatory system of interlinked signaling feedback loops controls mouse limb patterning. *Science* **323**, 1050-1053.

Benazet, J.-D., Pignatti, E., Nugent, A., Unal, E., Laurent, F. and Zeller, R. (2012). Smad4 is required to induce digit ray primordia and to initiate the aggregation and differentiation of chondrogenic progenitors in mouse limb buds. *Development* **139**, 4250-4260.

Bi, W., Deng, J. M., Zhang, Z., Behringer, R. R. and de Crombrugghe, B. (1999). Sox9 is required for cartilage formation. *Nat. Genet.* **22**, 85-89.

Boehm, B., Westerberg, H., Lesnicar-Pucko, G., Raja, S., Rautschka, M., Cotterell, J., Swoger, J. and Sharpe, J. (2010). The role of spatially controlled cell proliferation in limb bud morphogenesis. *PLoS Biol.* **8**, e1000420-e1000420.

Braem, K., Luyten, F. P. and Lories, R. J. U. (2012). Blocking p38 signalling inhibits chondrogenesis in vitro but not ankylosis in a model of ankylosing spondylitis in vivo. *Ann. Rheum. Dis.* **71**, 722-728.

Bragdon, B., Moseychuk, O., Saldanha, S., King, D., Julian, J. and Nohe, A. (2011). Bone morphogenetic proteins: a critical review. *Cell. Signal.* **23**, 609-620.

Brunet, L. J., McMahon, J. A., McMahon, A. P. and Harland, R. M. (1998). Noggin, cartilage morphogenesis, and joint formation in the mammalian skeleton. *Science* **280**, 1455-1457.

Buckland, R. A., Collinson, J. M., Graham, E., Davidson, D. R. and Hill, R. E. (1998). Antagonistic effects of FGF4 on BMP induction of apoptosis and chondrogenesis in the chick limb bud. *Mech. Dev.* **71**, 143-150.

Burgos, E. S., Wilczek, C., Onikubo, T., Bonanno, J. B., Jansong, J., Reimer, U. and Shechter, D. (2015). Histone H2A and H4 N-terminal tails are positioned by the MEP50 WD repeat protein for efficient methylation by the PRMT5 arginine methyltransferase. *J. Biol. Chem.* **290**, 9674-9689.

Byrnes, A. M., Racacho, L., Nikkel, S. M., Xiao, F., MacDonald, H., Underhill, T. M. and Bulman, D. E. (2010). Mutations in GDF5 presenting as semidominant brachydactyly A1. *Hum. Mutat.* **31**, 1155-1162.

Capdevila, J., Tsukui, T., Rodriquez Esteban, C., Zappavigna, V. and Belmonte, J. C. I. (1999). Control of vertebrate limb outgrowth by the proximal factor Meis2 and distal antagonism of BMPs by Gremlin. *Mol. Cell* **4**, 839-849.

Chari, A., Golas, M. M., Klingenhäger, M., Neuenkirchen, N., Sander, B., Englbrecht, C., Sickmann, A., Stark, H. and Fischer, U. (2008). An assembly chaperone collaborates with the SMN complex to generate spliceosomal SnRNPs. *Cell* **135**, 497-509.

Chen, J. C., Hsieh, M. J., Chen, C. J., Lin, J. T., Lo, Y. S., Chuang, Y. C., Chien, S. Y. and Chen, M. K. (2016). Polyphyllin G induce apoptosis and autophagy in human nasopharyngeal cancer cells by modulation of AKT and mitogen-activated protein kinase pathways in vitro and in vivo. *Oncotarget* **7**, 70276-70289.

Chiang, C., Litingtung, Y., Harris, M. P., Simandl, B. K., Li, Y., Beachy, P. A. and Fallon, J. F. (2001). Manifestation of the limb prepattern: limb development in the absence of Sonic hedgehog function. *Dev. Biol.* **236**, 421-435.

Cooper, K. L., Hu, J. K.-H., ten Berge, D., Fernandez-Teran, M., Ros, M. A. and Tabin, C. J. (2011). Initiation of proximal-distal patterning in the vertebrate limb by signals and growth. *Science* **332**, 1083-1086.

Cuadrado, A., Lafarga, V., Cheung, P. C. F., Dolado, I., Llanos, S., Cohen, P. and Nebreda, A. R. (2007). A new p38 MAP kinase-regulated transcriptional coactivator that stimulates p53-dependent apoptosis. *EMBO J.* **26**, 2115-2126.

Derynck, R. and Zhang, Y. E. (2003). Smad-dependent and Smad-independent pathways in TGF-β family signalling. *Nature* **425**, 577-584.

Dhar, S., Vemulapalli, V., Patananan, A. N., Huang, G. L., Di Lorenzo, A., Richard, S., Comb, M. J., Guo, A., Clarke, S. G. and Bedford, M. T. (2013). Loss of the major Type I arginine methyltransferase PRMT1 causes substrate scavenging by other PRMTs. *Sci. Rep.* **3**, 1311.

Di Lorenzo, A. and Bedford, M. T. (2011). Histone arginine methylation. *FEBS Lett.* **585**, 2024-2031.

Dudley, A. T., Ros, M. A. and Tabin, C. J. (2002). A re-examination of proximodistal patterning during vertebrate limb development. *Nature* **418**, 539-544.

Engel, F. B., Schebesta, M., Duong, M. T., Lu, G., Ren, S., Madwed, J. B., Jiang, H., Wang, Y. and Keating, M. T. (2005). p38 MAP kinase inhibition enables proliferation of adult mammalian cardiomyocytes. *Genes Dev.* **19**, 1175-1187.

Feng, X.-H. and Derynck, R. (2005). Specificity and versatility in tgf-beta signaling through Smads. *Annu. Rev. Cell Dev. Biol.* **21**, 659-693.

Fogel, J. L., Thein, T. Z. T. and Mariani, F. V. (2012). Use of LysoTracker to detect programmed cell death in embryos and differentiating embryonic stem cells. *J. Vis. Exp.* **68**, pii: 4254.

Fukuda, N., Saitoh, M., Kobayashi, N. and Miyazono, K. (2006). Execution of BMP-4-induced apoptosis by p53-dependent ER dysfunction in myeloma and B-cell hybridoma cells. *Oncogene* **25**, 3509-3517.

Ganan, Y., Macias, D., Duterque-Coquillaud, M., Ros, M. A. and Hurle, J. M. (1996). Role of TGF beta s and BMPs as signals controlling the position of the digits and the areas of interdigital cell death in the developing chick limb autopod. *Development* **122**, 2349-2357.

Gros, J., Hu, J. K.-H., Vinegoni, C., Feruglio, P. F., Weissleder, R. and Tabin, C. J. (2010). WNT5A/JNK and FGF/MAPK pathways regulate the cellular events shaping the vertebrate limb bud. *Curr. Biol.* **20**, 1993-2002.

Hay, E., Lemonnier, J., Fromigue, O. and Marie, P. J. (2001). Bone morphogenetic protein-2 promotes osteoblast apoptosis through a Smad-independent, protein kinase C-dependent signaling pathway. *J. Biol. Chem.* **276**, 29028-29036.

Hirose, Y., Katayama, M., Stokoe, D., Haas-Kogan, D. A., Berger, M. S. and Pieper, R. O. (2003). The p38 mitogen-activated protein kinase pathway links the DNA mismatch repair system to the G2 checkpoint and to resistance to chemotherapeutic DNA-methylating agents. *Mol. Cell. Biol.* **23**, 8306-8315.

Hsu, D. R., Economides, A. N., Wang, X., Eimon, P. M. and Harland, R. M. (1998). The Xenopus Dorsalizing factor gremlin identifies a novel family of secreted proteins that antagonize BMP activities. *Mol. Cell* **1**, 673-683.

Kaltcheva, M. M., Anderson, M. J., Harfe, B. D. and Lewandoski, M. (2016). BMPs are direct triggers of interdigital programmed cell death. *Dev. Biol.* **411**, 266-276.

Kendall, S. E., Battelli, C., Irwin, S., Mitchell, J. G., Glackin, C. A. and Verdi, J. M. (2005). NRAGE mediates p38 activation and neural progenitor apoptosis via the bone morphogenetic protein signaling cascade. *Mol. Cell. Biol.* **25**, 7711-7724.

Khokha, M. K., Hsu, D., Brunet, L. J., Dionne, M. S. and Harland, R. M. (2003). Gremlin is the BMP antagonist required for maintenance of Shh and Fgf signals during limb patterning. *Nat. Genet.* **34**, 303-307.

Kim, G.-Y., Park, J.-H., Kim, H., Lim, H.-J. and Park, H.-Y. (2016). Coronin 1B serine 2 phosphorylation by p38alpha is critical for vascular endothelial growth factor-induced migration of human umbilical vein endothelial cells. *Cell. Signal.* **28**, 1817-1825.

Kimura, N., Matsuo, R., Shibuya, H., Nakashima, K. and Taga, T. (2000). BMP2-induced apoptosis is mediated by activation of the TAK1-p38 kinase pathway that is negatively regulated by Smad6. *J. Biol. Chem.* **275**, 17647-17652.

Kondo, A., Tokuda, H., Matsushima-Nishiwaki, R., Kuroyanagi, G., Yamamoto, N., Mizutani, J., Kozawa, O. and Otsuka, T. (2014). Rho-kinase limits BMP-4-stimulated osteocalcin synthesis in osteoblasts: regulation of the p38 MAP kinase pathway. *Life Sci.* **96**, 18-25.

Kraus, P., Fraidenraich, D. and Loomis, C. A. (2001). Some distal limb structures develop in mice lacking Sonic hedgehog signalling. *Mech. Dev.* **100**, 45-58.

Kua, H.-Y., Liu, H., Leong, W. F., Li, L., Jia, D., Ma, G., Hu, Y., Wang, X., Chau, J. F. L., Chen, Y.-G. et al. (2012). c-Abl promotes osteoblast expansion by differentially regulating canonical and non-canonical BMP pathways and p16INK4a expression. *Nat. Cell Biol.* **14**, 727-737.

Kuroyanagi, G., Tokuda, H., Yamamoto, N., Matsushima-Nishiwaki, R., Mizutani, J., Kozawa, O. and Otsuka, T. (2015). Resveratrol amplifies BMP-4-stimulated osteoprotegerin synthesis via p38 MAP kinase in osteoblasts. *Mol. Med. Rep.* **12**, 3849-3854.

Lafont, J. E., Poujade, F. A., Pasdeloup, M., Neyret, P. and Mallein-Gerin, F. (2015). Hypoxia potentiates the BMP-2 driven COL2A1 stimulation in human articular chondrocytes via p38 MAPK. *Osteoarthritis Cartilage* **24**, 856-867.

Lallemand, Y. (2005). Analysis of Msx1; Msx2 double mutants reveals multiple roles for Msx genes in limb development. *Development* **132**, 3003-3014.

Lallemand, Y., Nicola, M. A., Ramos, C., Bach, A., Cloment, C. S. and Robert, B. (2005). Analysis of Msx1; Msx2 double mutants reveals multiple roles for Msx genes in limb development. *Development* **132**, 3003-3014.

Lee, J. and Bedford, M. T. (2002). PABP1 identified as an arginine methyltransferase substrate using high-density protein arrays. *EMBO Rep.* **3**, 268-273.

Lefebvre, V. and Smits, P. (2005). Transcriptional control of chondrocyte fate and differentiation. *Birth Defects Res. C Embryo Today* **75**, 200-212.

Lehmann, K., Seemann, P., Stricker, S., Sammar, M., Meyer, B., Suring, K., Majewski, F., Tinschert, S., Grzeschik, K.-H., Muller, D. et al. (2003). Mutations in bone morphogenetic protein receptor 1B cause brachydactyly type A2. *Proc. Natl. Acad. Sci. USA* **100**, 12277-12282.

Lehmann, K., Seemann, P., Silan, F., Goecke, T. O., Irgang, S., Kjaer, K. W., Kjaergaard, S., Mahoney, M. J., Morlot, S., Reissner, C. et al. (2007). A new subtype of brachydactyly type B caused by point mutations in the bone morphogenetic protein antagonist NOGGIN. *Am. J. Hum. Genet.* **81**, 388-396.

Lewandowski, J. P., Pursell, T. A., Rabinowitz, A. H. and Vokes, S. A. (2014). Manipulating gene expression and signaling activity in cultured mouse limb bud cells. *Dev. Dyn.* **243**, 928-936.

Lo, R. S., Wotton, D. and Massagué, J. (2001). Epidermal growth factor signaling via Ras controls the Smad transcriptional co-repressor TGIF. *EMBO J.* **20**, 128-136.

Logan, M., Martin, J. F., Nagy, A., Lobe, C., Olson, E. N. and Tabin, C. J. (2002). Expression of Cre recombinase in the developing mouse limb bud driven by a Prxl enhancer. *Genesis* **33**, 77-80.

Lopez-Rios, J., Speziale, D., Robay, D., Scotti, M., Osterwalder, M., Nusspaumer, G., Galli, A., Holländer, G. A., Kmita, M. and Zeller, R. (2012). GLI3 constrains digit number by controlling both progenitor proliferation and BMP-dependent exit to chondrogenesis. *Dev. Cell* **22**, 837-848.

Lu, P. (2006). Increasing Fgf4 expression in the mouse limb bud causes polysyndactyly and rescues the skeletal defects that result from loss of Fgf8 function. *Development* **133**, 33-42.

Macias, D., Gañan, Y., Sampath, T. K., Piedra, M. E., Ros, M. A. and Hurle, J. M. (1997). Role of BMP-2 and OP-1 (BMP-7) in programmed cell death and skeletogenesis during chick limb development. *Development* **124**, 1109-1117.

Mariani, F. V., Ahn, C. P. and Martin, G. R. (2008). Genetic evidence that FGFs have an instructive role in limb proximal–distal patterning. *Nature* **453**, 401-405.

Meister, G. and Fischer, U. (2002). Assisted RNP assembly: SMN and PRMT5 complexes cooperate in the formation of spliceosomal UsnRNPs. *EMBO J.* **21**, 5853-5863.

Merino, R., Gañán, Y., Macias, D., Rodríguez-León, J. and Hurle, J. M. (1999a). Bone morphogenetic proteins regulate interdigital cell death in the avian embryo. *Ann. N. Y. Acad. Sci.* **887**, 120-132.

Merino, R., Macias, D., Gañan, Y., Economides, A. N., Wang, X., Wu, Q., Stahl, N., Sampath, K. T., Varona, P. and Hurle, J. M. (1999b). Expression and function of Gdf-5 during digit skeletogenesis in the embryonic chick leg bud. *Dev. Biol.* **206**, 33-45.

Michos, O., Panman, L., Vintersten, K., Beier, K., Zeller, R. and Zuniga, A. (2004). Gremlin-mediated BMP antagonism induces the epithelial-mesenchymal feedback signaling controlling metanephric kidney and limb organogenesis. *Development* **131**, 3401-3410.

Montero, J. A., Lorda-Diez, C. I., Gañan, Y., Macias, D. and Hurle, J. M. (2008). Activin/TGFbeta and BMP crosstalk determines digit chondrogenesis. *Dev. Biol.* **321**, 343-356.

Nagamatsu, G., Kosaka, T., Kawasumi, M., Kinoshita, T., Takubo, K., Akiyama, H., Sudo, T., Kobayashi, T., Oya, M. and Suda, T. (2011). A germ cell-specific gene, Prmt5, works in somatic cell reprogramming. *J. Biol. Chem.* **286**, 10641-10648.

Nakamura, K., Shirai, T., Morishita, S., Uchida, S., Saeki-Miura, K. and Makishima, F. (1999). p38 mitogen-activated protein kinase functionally contributes to chondrogenesis induced by growth/differentiation factor-5 in ATDC5 cells. *Exp. Cell Res.* **250**, 351-363.

Neuenkirchen, N., Englbrecht, C., Ohmer, J., Ziegenhals, T., Chari, A. and Fischer, U. (2015). Reconstitution of the human U snRNP assembly machinery reveals stepwise Sm protein organization. *EMBO J.* **34**, 1925-1941.

Norrie, J. L., Lewandowski, J. P., Bouldin, C. M., Amarnath, S., Li, Q., Vokes, M. S., Ehrlich, L. I. R., Harfe, B. D. and Vokes, S. A. (2014). Dynamics of BMP signaling in limb bud mesenchyme and polydactyly. *Dev. Biol.* **393**, 270-281.

Pajni-Underwood, S., Wilson, C. P., Elder, C., Mishina, Y. and Lewandoski, M. (2007). BMP signals control limb bud interdigital programmed cell death by regulating FGF signaling. *Development* **134**, 2359-2368.

Paulsen, D. F. and Solursh, M. (1988). Microtiter micromass cultures of limb-bud mesenchymal cells. *In Vitro Cell. Dev. Biol.* **24**, 138-147.

Pelz, J.-P., Schindelin, H., van Pee, K., Kuper, J., Kisker, C., Diederichs, K., Fischer, U. and Grimm, C. (2015). Crystallizing the 6S and 8S spliceosomal assembly intermediates: a complex project. *Acta Crystallogr. Sect. D Biol. Crystallogr.* **71**, 2040-2053.

Pizette, S. and Niswander, L. (1999). BMPs negatively regulate structure and function of the limb apical ectodermal ridge. *Development* **126**, 883-–8894.

Pizette, S. and Niswander, L. (2000). BMPs are required at two steps of limb chondrogenesis: formation of prechondrogenic condensations and their differentiation into chondrocytes. *Dev. Biol.* **219**, 237-249.

Pizette, S., Abate-Shen, C. and Niswander, L. (2001). BMP controls proximodistal outgrowth, via induction of the apical ectodermal ridge, and dorsoventral patterning in the vertebrate limb. *Development* **128**, 4463-4474.

Ploger, F., Seemann, P., Schmidt-von Kegler, M., Lehmann, K., Seidel, J., Kjaer, K. W., Pohl, J. and Mundlos, S. (2008). Brachydactyly type A2 associated with a defect in proGDF5 processing. *Hum. Mol. Genet.* **17**, 1222-1233.

Robertson, E. J., Charatsi, I., Joyner, C. J., Koonce, C. H., Morgan, M., Islam, A., Paterson, C., Lejsek, E., Arnold, S. J., Kallies, A. et al. (2007). Blimp1 regulates development of the posterior forelimb, caudal pharyngeal arches, heart and sensory vibrissae in mice. *Development* **134**, 4335-4345.

Rosello-Diez, A., Arques, C. G., Delgado, I., Giovinazzo, G. and Torres, M. (2014). Diffusible signals and epigenetic timing cooperate in late proximo-distal limb patterning. *Development* **141**, 1534-1543.

Saha, K., Adhikary, G. and Eckert, R. L. (2016). MEP50/PRMT5 reduces gene expression by histone arginine methylation and this is reversed by PKCδ/p38δ signaling. *J. Invest. Dermatol.* **136**, 214-224.

Saiz-Lopez, P., Chinnaiya, K., Campa, V. M., Delgado, I., Ros, M. A. and Towers, M. (2015). An intrinsic timer specifies distal structures of the vertebrate limb. *Nat. Commun.* **6**, 8108.

Sapkota, G., Alarcón, C., Spagnoli, F. M., Brivanlou, A. H. and Massagué, J. (2007). Balancing BMP signaling through integrated inputs into the Smad1 linker. *Mol. Cell* **25**, 441-454.

Shubin, N. H. and Alberch, P. (1986). A morphogenetic approach to the origin and basic organization of the tetrapod limb. In *Evolutionary Biology*, Vol. 20 (ed. M. K. Hecht, B. Wallace and G. T. Prance), pp. 319-387. Boston, MA: Springer.

Stark, R. J. and Searls, R. L. (1973). A description of chick wing bud development and a model of limb morphogenesis. *Dev. Biol.* **33**, 138-153.

Stopa, N., Krebs, J. E. and Shechter, D. (2015). The PRMT5 arginine methyltransferase: many roles in development, cancer and beyond. *Cell. Mol. Life Sci.* **72**, 2041-2059.

Development (2016) 143, 4608-4619 doi:10.1242/dev.140715

Storey, J. D. and Tibshirani, R. (2003). Statistical significance for genomewide studies. *Proc. Natl. Acad. Sci. USA* **100**, 9440-9445.

Storm, E. E. and Kingsley, D. M. (1999). GDF5 coordinates bone and joint formation during digit development. *Dev. Biol.* **209**, 11-27.

Sun, X., Mariani, F. V. and Martin, G. R. (2002). Functions of FGF signalling from the apical ectodermal ridge in limb development. *Nature* **418**, 501-508.

Suzuki, T., Hasso, S. M. and Fallon, J. F. (2008). Unique SMAD1/5/8 activity at the phalanx-forming region determines digit identity. *Proc. Natl. Acad. Sci. USA* **105**, 4185-4190.

Tee, W.-W., Pardo, M., Theunissen, T. W., Yu, L., Choudhary, J. S., Hajkova, P. and Surani, M. A. (2010). Prmt5 is essential for early mouse development and acts in the cytoplasm to maintain ES cell pluripotency. *Genes Dev.* **24**, 2772-2777.

ten Berge, D., Brugmann, S. A., Helms, J. A. and Nusse, R. (2008). Wnt and FGF signals interact to coordinate growth with cell fate specification during limb development. *Development* **135**, 3247-3257.

Thorogood, P. V. and Hinchliffe, J. R. (1975). An analysis of the condensation process during chondrogenesis in the embryonic chick hind limb. *J. Embryol. Exp. Morphol.* **33**, 581-606.

Tian, X. Y., Yung, L. H., Wong, W. T., Liu, J., Leung, F. P., Liu, L., Chen, Y., Kong, S. K., Kwan, K. M., Ng, S. M. et al. (2012). Bone morphogenic protein-4 induces endothelial cell apoptosis through oxidative stress-dependent p38MAPK and JNK pathway. *J. Mol. Cell. Cardiol.* **52**, 237-244.

Tong, L., Pav, S., White, D. M., Rogers, S., Crane, K. M., Cywin, C. L., Brown, M. L. and Pargellis, C. A. (1997). A highly specific inhibitor of human p38 MAP kinase binds in the ATP pocket. *Nat. Struct. Biol.* **4**, 311-316.

Trapnell, C., Roberts, A., Goff, L., Pertea, G., Kim, D., Kelley, D. R., Pimentel, H., Salzberg, S. L., Rinn, J. L. and Pachter, L. (2012). Differential gene and transcript expression analysis of RNA-seq experiments with TopHat and Cufflinks. *Nat. Protoc.* **7**, 562-578.

Wang, Y., Zhou, X., Oberoi, K., Phelps, R., Couwenhoven, R., Sun, M., Rezza, A., Holmes, G., Percival, C. J., Friedenthal, J. et al. (2012). p38 Inhibition ameliorates skin and skull abnormalities in Fgfr2 Beare-Stevenson mice. *J. Clin. Invest.* **122**, 2153-2164.

Wang, J., Duncan, D., Shi, Z. and Zhang, B. (2013). WEB-based GEne SeT AnaLysis Toolkit (WebGestalt): update 2013. *Nucleic Acids Res.* **41**, W77-W83.

Witte, F., Chan, D., Economides, A. N., Mundlos, S. and Stricker, S. (2010). Receptor tyrosine kinase-like orphan receptor 2 (ROR2) and Indian hedgehog regulate digit outgrowth mediated by the phalanx-forming region. *Proc. Natl. Acad. Sci. USA* **107**, 14211-14216.

Worthley, D. L., Churchill, M., Compton, J. T., Tailor, Y., Rao, M., Si, Y., Levin, D., Schwartz, M. G., Uygur, A., Hayakawa, Y. et al. (2015). Gremlin 1 identifies a skeletal stem cell with bone, cartilage, and reticular stromal potential. *Cell* **160**, 269-284.

Wright, E., Hargrave, M. R., Christiansen, J., Cooper, L., Kun, J., Evans, T., Gangadharan, U., Greenfield, A. and Koopman, P. (1995). The Sry-related gene Sox9 is expressed during chondrogenesis in mouse embryos. *Nat. Genet.* **9**, 15-20.

Zhang, B., Dong, S., Zhu, R., Hu, C., Hou, J., Li, Y., Zhao, Q., Shao, X., Bu, Q., Li, H. et al. (2015). Targeting protein arginine methyltransferase 5 inhibits colorectal cancer growth by decreasing arginine methylation of eIF4E and FGFR3. *Oncotarget* **6**, 22799-22811.

Zhao, Q., Rank, G., Tan, Y. T., Li, H., Moritz, R. L., Simpson, R. J., Cerruti, L., Curtis, D. J., Patel, D. J., Allis, C. D. et al. (2009). PRMT5-mediated methylation of histone H4R3 recruits DNMT3A, coupling histone and DNA methylation in gene silencing. *Nat. Struct. Mol. Biol.* **16**, 304-311.

Zhu, J., Nakamura, E., Nguyen, M.-T., Bao, X., Akiyama, H. and Mackem, S. (2008). Uncoupling sonic hedgehog control of pattern and expansion of the developing limb bud. *Dev. Cell* **14**, 624-632.